Chemical Engineering Journal 172 (2011) 258–266

Contents lists available at ScienceDirect

Chemical Engineering Journal

journal homepage: www.elsevier.com/locate/cej

Green synthesis of iron nanoparticles and their application as a Fenton-like catalyst for the degradation of aqueous cationic and anionic dyes

T. Shahwan[a,*], S. Abu Sirriah[a], M. Nairat[a], E. Boyacı[b], A.E. Eroğlu[b], T.B. Scott[c], K.R. Hallam[c]

[a] Department of Chemistry, Birzeit University, Ramalla, West Bank, Palestine
[b] Department of Chemistry, Izmir Institute of Technology, Urla 35430, Izmir, Turkey
[c] Interface Analysis Centre, University of Bristol, 121 St. Michael's Hill, Bristol BS2 8BS, United Kingdom

ARTICLE INFO

Article history:
Received 18 March 2011
Received in revised form 30 May 2011
Accepted 30 May 2011

Keywords:
Green synthesis
Iron nanoparticles
Methylene blue
Methyl orange
Fenton catalyst

ABSTRACT

Iron nanoparticles were produced using extracts of green tea leaves (GT-Fe NPs). The materials were characterized using TEM, SEM/EDX, XPS, XRD, and FTIR techniques and were shown to contain mainly iron oxide and iron oxohydroxide. The obtained nanoparticles were then utilized as a Fenton-like catalyst for decolorization of aqueous solutions containing methylene blue (MB) and methyl orange (MO) dyes. The related experiments investigated the removal kinetics and the effect of concentration for both MB and MO. The concentrations of dyes in aqueous solution were monitored using ultraviolet–visible (UV–vis) spectroscopy. The results indicated fast removal of the dyes with the kinetic data of MB following a second order removal rate, while those of MO were closer to a first order removal rate. The loading experiments indicated almost complete removal of both dyes from water over a wide range of concentration, 10–200 mg L^{-1}. Compared with iron nanoparticles produced by borohydride reduction, GT-Fe nanoparticles demonstrated more effective capability as a Fenton-like catalyst, both in terms of kinetics and percentage removal.

1. Introduction

Nanoscale iron particles are recently gaining great interest in environmental remediation circles. One of the prominent applications in this regard is the removal of organic and inorganic pollutants from aqueous solutions [1–8]. Iron nanoparticles containing iron oxides and zero valent iron (ZVI) can be used as a Fenton-like catalyst for the degradation of aqueous organic solutes [9–11]. The nano-scale size offers high surface area and high surface reactivity.

Iron nanoparticles can be readily synthesized using sodium borohydride, $NaBH_4$, as a reducing agent [12]. Various chemical and physical methods are being applied to obtain iron nanoparticles of specific sizes and morphologies. The aggregation of these nanoparticles into chain-like structures is one of their well known characteristics, which is responsible for reducing the surface area to volume ratio. The stability of iron nanoparticles against aggregation can be improved by imparting electrostatic repulsion, applying organic surfactants, or through the use of capping agents [13]. Another approach that would serve this goal is to synthesize iron nanoparticles in the presence of supporting inorganic material [14–16].

Green synthesis of iron nanoparticles is evolving as a method that would impart steric stabilization of iron nanoparticles against aggregation, and help overcome the concerns related with using sodium borohydride as a reducing agent in routine synthesis reported so far. This chemical is known for its corrosiveness and flammability [17]. Recently, successful synthesis of iron nanoparticles utilizing green tea leaf and sorghum bran extracts have been reported [17–19].

In this work, iron nanoparticles were readily synthesized using green tea leaf extracts (GT-Fe NPs). Green tea is known to contain polyphenols that act both as a reducing agent and a capping agent. The synthesis and applicability of the material in the effective removal of bromothylmol blue has been reported [17]. The main objective of the current study is to test the applicability of GT-Fe NPs as a Fenton catalyst in the removal of cationic (methylene blue) and anionic (methyl orange) model dyes. Another objective of the study is to compare the extent of degradation of GT-Fe NPs with that of nZVI produced by borohydride reduction (BH–Fe NPs). The produced GT-Fe NPs were characterized using TEM, SEM/EDX, XPS, XRD, and FTIR. The oxidative decolorization, using H_2O_2, was studied over a wide range of periods of contact and concentrations of aqueous solutions of methylene blue (MB) and methyl orange (MO). Methylene blue is a heterocyclic aromatic chemical compound with the molecular formula $C_{16}H_{18}N_3SCl$ (Fig. 1a). At room temperature

* Corresponding author.
E-mail addresses: tshahwan@birzeit.edu, talalshahwan@iyte.edu.tr (T. Shahwan).

1385-8947/$ – see front matter © 2011 Elsevier B.V. All rights reserved.
doi:10.1016/j.cej.2011.05.103

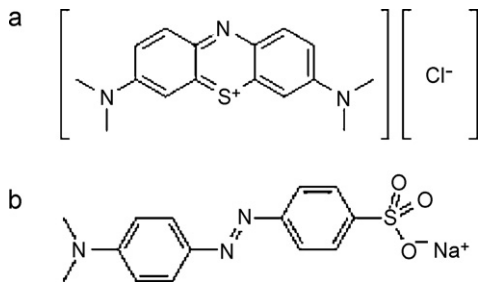

Fig. 1. The structural formula for: (a) methylene blue, and (b) methyl orange, salts.

it appears as a solid, odorless, dark green powder, which yields a blue solution when dissolved in water. Methyl orange (Fig. 1b) is an anionic dye with the formula $C_{14}H_{14}N_3NaO_3S$ which is usually chosen as one of the model azo dyes in literature. Azo dyes are a major class of synthetic, colored organic compounds that account for about half of the textile dyestuffs used today [20].

2. Experimental

2.1. Preparation of GT-Fe NPs

The synthesis of iron nanoparticles using green tea extracts was described previously [17,18]. In this work, the green tea extract was prepared by heating 60.0 g L^{-1} green tea (Alwald Brand) until boiling. After settling for 1.0 h, the extract was vacuum-filtered. Separately, a solution of 0.10 M $FeCl_2{\cdot}4H_2O$ was prepared by adding 19.9 g of solid $FeCl_2{\cdot}4H_2O$ (Aldrich 22029-9) in 1.0 L of deionized water. Subsequently, 0.10 M $FeCl_2{\cdot}4H_2O$ solution was added to 60.0 g L^{-1} green tea in 2:3 volume ratio. Following this, 1.0 M NaOH solution was added until the pH was 6.0 and the formation of GT-Fe NPs was marked by the appearance of intense black precipitate. The iron particles were then separated first by evaporating water from the iron solution on a hot plate (Freed Electric), and then by drying it overnight in a fume hood.

2.2. Preparation of methylene blue, methyl orange, and H_2O_2 solutions

1000.0 mg L^{-1} stock solutions of MB (Certistain 15943) and MO (Aldrich 140910) were first prepared. Less concentrated solutions were then obtained by serial dilution using deionized water. Separately, a 10.0% H_2O_2 solution (v/v) was prepared from a stock 30.0% H_2O_2 solution (Merck 64271) by dilution with deionized water.

2.3. Decolorization experiments

All the decolorization experiments were carried out under atmospheric pressure, by shaking Erlenmeyer flasks in a thermostat water bath that was adjusted to 25 °C for all experiments. The UV–vis absorbance readings were taken using a Varian Carry 50 spectrophotometer at λ_{max} = 665 nm for MB, and λ_{max} = 465 nm for MO. The concentrations were determined using the calibration curves for both dyes. In addition, parallel blank experiments were carried out under the same conditions, with just H_2O_2 solution and without GT-Fe NPs, to assess the capability of H_2O_2 alone in dye degradation.

In the kinetic experiments, 50.0 mg of GT-Fe NPs were added to solutions containing 5.0 mL of 10.0% H_2O_2 and 45.0 mL of 50.0 mg L^{-1} dye solutions. This mixture was placed in 50.0 mL polypropylene tubes, and shaken in a water bath. The solutions were then separated from the GT-Fe NPs by simple decantation. Subsequently, the UV–vis absorbance readings were obtained after different times of contact (5.0 min, 30.0 min, 60.0 min, 120.0 min, 200.0 min, 300.0 min, and 360.0 min).

To determine the effect of dye concentration on the extent of degradation, 50.0 mL portions of different concentrations (10.0, 25.0, 50.0, 100.0, and 200.0 mg L^{-1}) for each dye were mixed with 10.0 mL of 10.0% H_2O_2 and 50.0 mg of GT-Fe NPs. The reactions were performed in 100.0 mL Erlenmeyer flasks, which were placed in a water bath for 6 h. Finally, the solutions were filtered and the dye concentrations were measured using UV–vis spectrophotometry.

2.4. Characterization of GT-Fe NPs

The synthesized GT-Fe NPs were characterized using TEM, XPS, SEM/EDX, XRD and FTIR techniques.

A Philips X'Pert Pro instrument was used for the XRD analysis. The source consisted of Cu K_α radiation (λ = 1.54 Å). Each sample was scanned within the 2θ range of 20–70°. The samples of GT-Fe NPs were repeatedly washed with ethanol prior to XRD analysis to reduce the NaCl content that crystallized out during the synthesis process.

SEM/EDX analysis was carried out using a Philips XL-30S FEG type instrument. The GT-Fe NPs were sprinkled onto adhesive carbon tapes supported on metallic disks, and their images and elemental contents were recorded at different magnifications.

FTIR analysis was carried out for GT-Fe NPs before and after the degradation experiments. The spectra were acquired by direct analysis of GT-Fe NPs using a Varian Carry 50 spectrophotometer.

For XPS, samples were analyzed under high vacuum using a Thermo Fisher Scientific Escascope X-ray photoelectron spectrometer equipped with a dual anode (Mg/Al) source and a concentric hemispherical electron energy analyzer. Al K_α radiation at 400 W (15 kV; 26 mA) was utilized. During acquisition of spectra, the pressure in the main chamber was maintained at $<1 \times 10^{-8}$ mbar to ensure a clean sample surface. Data acquisition and manipulation were carried out using Pisces (Dayta Systems, UK) software. Charge referencing was carried out against adventitious hydrocarbon (C 1s = 284.8 eV binding energy). TEM images were obtained with a JEOL JEM 1200 EX Mk 2 TEM, operating at 120 keV. Nanoparticle samples were sonicated in analytical grade methanol for 30 s and mounted on 200 mesh holey carbon coated copper grids.

3. Results and discussion

3.1. Characterization of GT-Fe NPs

TEM images in addition to an EDX spectrum of GT-Fe NPs are shown in Fig. 2. The GT-Fe NPs tend to form irregular clusters but also demonstrate some dispersion, with particle size ranging roughly between 40 nm and 60 nm. The EDX spectrum (Fig. 2c) contains intense peaks of C, Na, and Cl in addition to Fe and O. The Na and Cl signals must be originating from NaOH and $FeCl_2$ precursors used in the synthesis of GT-Fe NPs. The C signals are attributed mainly to the polyphenol groups and other C-containing molecules in the green tea extracts. The atomic percentages as obtained by EDX quantification were 47.9% C, 6.3% O, 12.5% Na, 5.5% Cl, and 27.8% Fe. These values could be helpful in reflecting the atomic content on the surface and near surface regions of the NPs.

The structure of the material was characterized also by XRD after exposing the sample to repetitive washings with ethanol to reduce the amount of NaCl crystals. The reflections in the diagram (Fig. 3) were identified to belong to iron oxide (Fe_3O_4) [21], and iron oxohydroxide (FeOOH) [22], in addition to NaCl. Our previous investigations of nZVI produced by borohydride reduction indicate that Fe^0 is of the α-Fe crystalline type [15]. However, recent reports indicate that Fe^0 produced by reduction with green tea [17] and sorghum bran [19] extracts is amorphous in nature, possibly

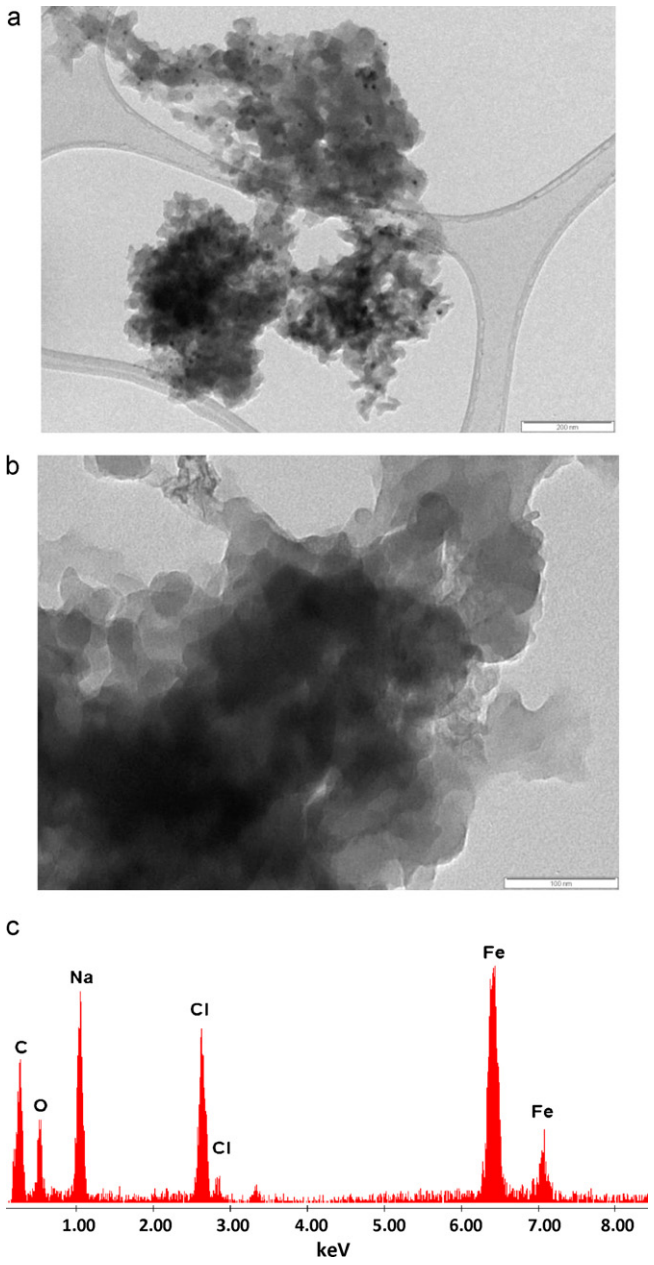

Fig. 2. (a and b) TEM images, and (c) EDX spectrum, of GT-Fe NPs.

explaining the absence of diffraction lines of Fe^0 in our samples. Nevertheless, the formation of hexagonal Fe^0 in some iron samples was also noted [17].

XPS spectra of GT-Fe NPs are shown in Fig. 4. The same elements appearing in the EDX spectrum are also observed using XPS spectra. Auger electron peaks are observed for Na and O in addition to their photoelectron peaks. The photoelectron profiles for Fe 2p, O 1s, and C 1s are shown in the insets in Fig. 4. The O 1s profile contains two shoulders at 530.4 eV and 531.6 eV, in addition to 532.8 eV. These features can be attributed, respectively, to O in the iron oxide lattice [23], O in structural OH^- [24], and O in physisorbed water [25]. The C 1s profile shows a duplet at 285.2 eV and 286.4 eV. These signals are thought to arise primarily from the C atoms in the polyphenol groups attached to GT-Fe NPs, with the duplet indicating two types of C with different chemical environments. The Fe 2p profile contains the characteristic $2p_{3/2}$ and $2p_{1/2}$ peaks centered at 711.5 eV and 725.2 eV, respectively. The energy corresponding to Fe $2p_{3/2}$ is typical for iron in iron oxide [26] and in iron oxohydroxide [24].

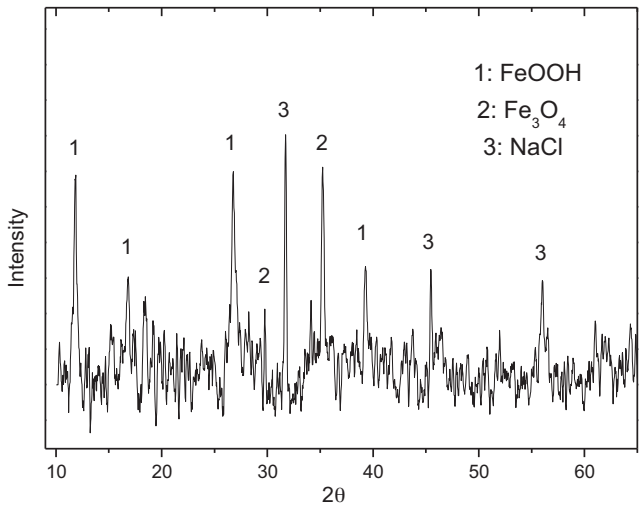

Fig. 3. A typical XRD pattern of GT-Fe NPs.

FTIR spectra of GT-Fe NPs revealed several peaks in the spectral range 800–1800 cm^{-1} (Fig. 5a). These peaks are attributed to the polyphenols presumably present at the surface of iron nanoparticles. A very strong peak at 1065 cm^{-1} relates to the stretching vibration of C–O–C, and that around 1220 cm^{-1} is ascribed to the asymmetric stretching bands. The features around 1400 cm^{-1} correspond to the in-plane bending vibrations of –OH in phenols. Moreover, the peak around 1600 cm^{-1} can be attributed to the C=C ring stretching in polyphenols [27]. As can be seen in the figure, these peaks disappeared after GT-Fe NPs material was contacted with MB and MO solutions, most probably under the action of hydroxyl radicals, as discussed in the next section.

3.2. MB and MO degradation experiments

3.2.1. Fenton-like mechanism and pH effect

Chemical oxidation of organic molecules is a powerful method for the degradation of pollutants from contaminated water. The oxidation is based on the action of hydroxyl radical ($OH^•$), generated in aqueous solution by the well known Fenton reagent which is a combination of Fe^{2+} and hydrogen peroxide, H_2O_2, in aqueous solution [20]. In a Fenton-like process, a solid iron mineral can be used to replace the dissolved iron (Fe^{2+}) used in traditional Fenton processes [28]. The disadvantages of the traditional Fenton process include the production of large amounts of sludge and the formation of a high concentration of anions in the treated wastewater [20]. Unlike the traditional Fenton's reagent where the pH values have to be lowered below 4, the reaction between iron bearing minerals and hydrogen peroxide can effectively oxidize the organic molecules at circumneutral pH [28].

In a classical Fenton system, the generation cycle of hydroxyl radicals can be represented by:

$$Fe^{2+} + H_2O_2 \rightarrow Fe^{3+} + OH^• + OH^- \quad \text{(i)}$$

$$Fe^{3+} + H_2O_2 \rightarrow Fe^{2+} + OOH^• + H^+ \quad \text{(ii)}$$

Eqs. (i) and (ii) show that ferrous ions initiate the reaction leading to production of hydroxyl radicals, which then attack the organic pollutants leading to their degradation. Iron oxides, iron oxohydroxide, and zero valent iron can be used as a source of ferrous ions in a Fenton-like process. These materials have been employed to catalyze degradation of dye pollutants and other organic pollutants [9–11,14,16,20,29]. In this study, the synthesized GT-Fe NPs were shown to contain mainly iron oxide and iron oxohydroxide. The sustainability of the hydroxyl generation cycle

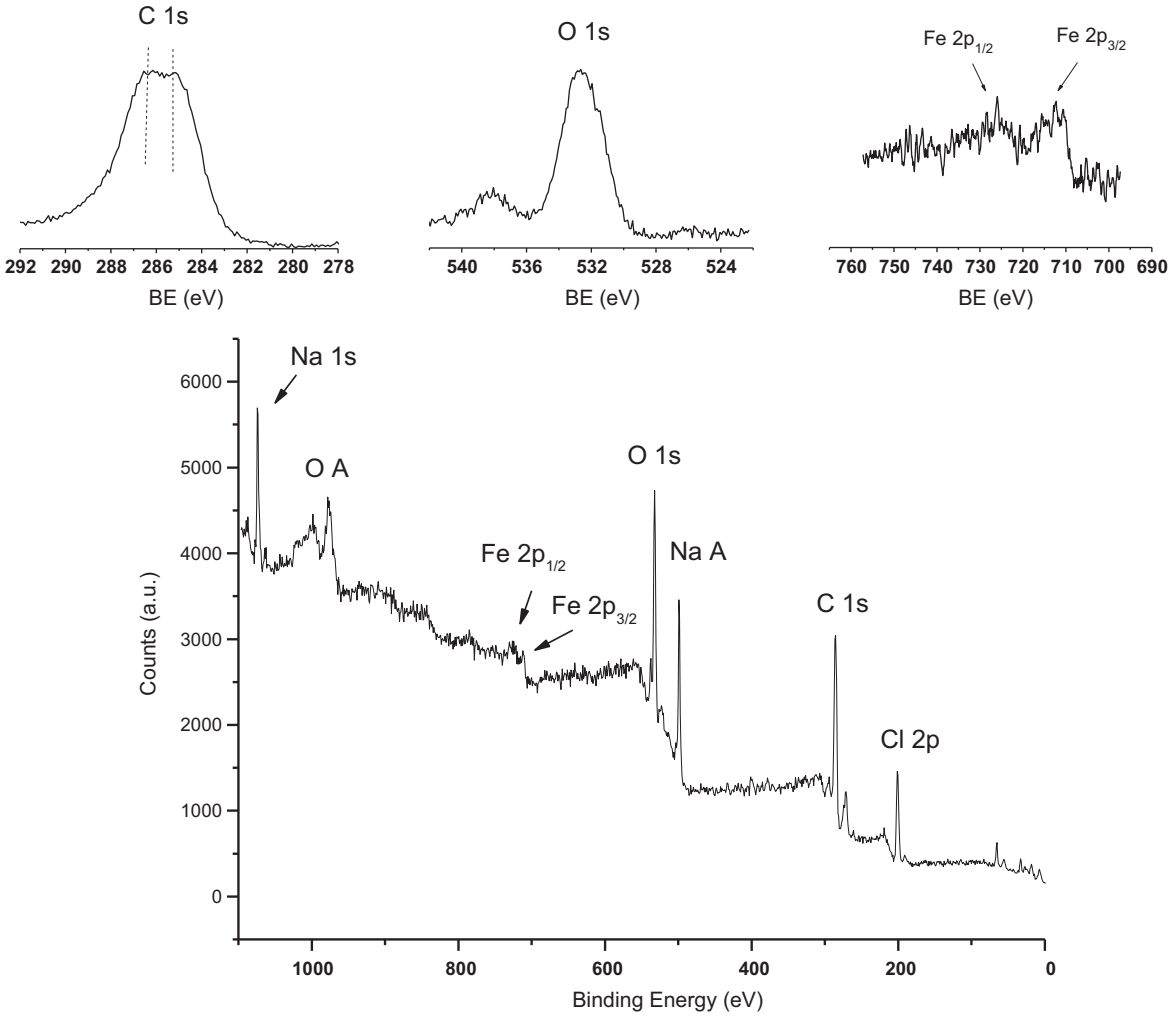

Fig. 4. XPS spectra of GT-Fe NPs. The insets show the peaks corresponding to C 1s, O 1s and Fe 2p.

(Eqs. (i)–(ii)) will thus depend on the ease of ferrous ion availability. In this sense, acidity is a crucial factor for the Fenton oxidation system. In acidic solution, the surface of the iron oxide/oxohydroxide corrodes producing ferrous ions, which in turn generate the OH• radicals. These radicals attack bonds in the dye molecules which might be in solution or sorbed on the catalyst surface [28]. For example, in the case of azo dyes, the cleavage of the azo bond (–N=N–) in the chromophore of the dye leads to decolorization of the dye solution [20]. The sorption rate could be a controlling factor of the whole catalytic oxidation reaction [30]. In this sense, the surface area and surface activity of the Fenton catalyst are crucial. Crystallinity, iron content, and oxidation state of iron are also considered as important factors in determining the activity of the iron oxide used as a Fenton-like catalyst [28]. Doubtlessly, the nanosize of the GT-Fe material greatly enhances its activity as a catalyst. Moreover, the relatively weak and broad peaks in the XRD diagram (Fig. 3) indicate that the material has amorphous grains, a factor that will facilitate its dissolution under the acid attack. It is reported that the generation of ferrous ions increases with a decrease in pH [29], and as shown in the next sections, the medium of the reaction during the decolorization experiments was quite acidic (pH 3.0–3.3).

3.2.2. FTIR analysis

FTIR spectra were recorded for GT-Fe NPs before and after the degradation reactions of MB and MO dyes. The spectra obtained for GT-Fe NPs after contact with MB solution showed spectral features at 2925 cm^{-1} and 2818 cm^{-1} (Fig. 5b). These bands relate to the stretching vibration of C–H in the methyl groups, originating from MB and/or its degradation products adsorbed on the iron nanoparticles surface [31].

The spectra obtained for GT-Fe NPs after contact with MO solution indicate the appearance of a feature at 2927 cm^{-1} (Fig. 5c), that relates to asymmetric $-CH_3$ vibrations. In addition, other peaks were observed at 697 cm^{-1}, 629 cm^{-1}, and 572 cm^{-1} that are attributed to –C–S– stretching vibrations [32]. These features show that MO and/or its degradation products were attached to the GT-Fe NPs surface.

3.2.3. Kinetic experiments

The variation of MB and MO concentration with time are shown in Fig. 6a and b. The insets show the reduction in the intensity of the UV–vis absorption spectra of the dyes with time. It is worth mentioning that the spectral bands showed shifts due to the acidity of the medium. The UV–vis band of MB monomer in water appears normally at 665 nm. Aggregation of the dye leads to red or blue shifts depending on the type of aggregate. In this study, the MB bands were centered around 590 nm, which are attributed to dye aggregation in the acidic medium. Such blue shifts were also recorded in basic medium but were suggested to arise from demethylation of the dye molecules rather than their aggregation [33]. The spectral band of MO is known to appear at 465 nm. In this

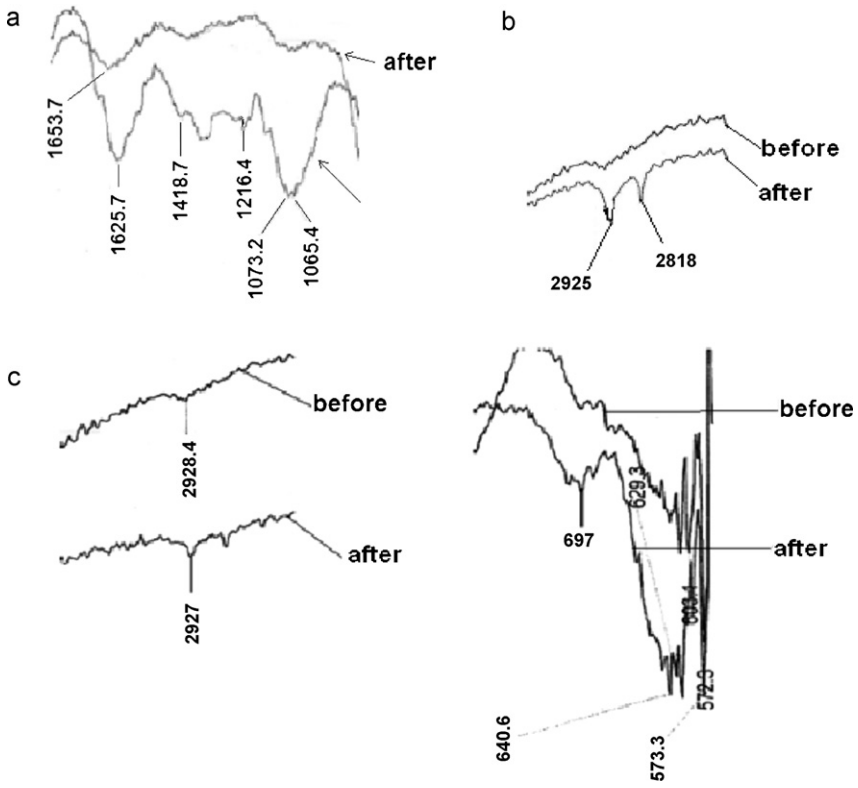

Fig. 5. FTIR bands corresponding to: (a) polyphenols, (b) MB, and (c) MO. The spectra were recorded for GT-Fe NPs before and after exposure to MB and MO dyes.

work, the spectral band of MO is red shifted to 505–510 nm. Such a shift is reported to occur when the pH is below 5, and to result from protonation of the MO molecules to form azonium ion on the molecular structure [34].

No pH control was performed during the decolorization experiments. Before adding the H_2O_2 solutions, the pH of MB solution (containing GT-Fe NPs) was 8.31, and that of MO solution was 8.30. As soon as the peroxide solution was added to MB solution, the pH decreased to 3.10 and continued to more slowly decrease until it reached 3.02 at the end of the experiment (after 6 h of contact). On the other hand, when the peroxide solution was added to the MO solution, the pH decreased to 3.27 and continued to steadily decrease until it reached 3.11 at the end of the shaking time. In both cases, the decrease in pH was accompanied with an increase in the conductance of the solution which was around 0.01 mS before the addition of the peroxide, and increased steadily to about 0.70 mS at the end of the experiments. The pH values measured in this study are below 4.0, which is important for the generation of hydroxyl radical. It is suggested that at pH above 4, the generation of hydroxyl radicals becomes slower due to the formation of the ferric–hydroxo complexes, thus reducing the efficiency of the Fenton system [35].

It is clear from Fig. 6 that the removal of MB proceeds almost instantaneously, with more than 80% of the dye being removed within the first 5 min of operation. Comparatively, the removal of MO is slower, with 80% of the dye being removed after about 1 h of operation. Almost complete removal of the dyes can be achieved

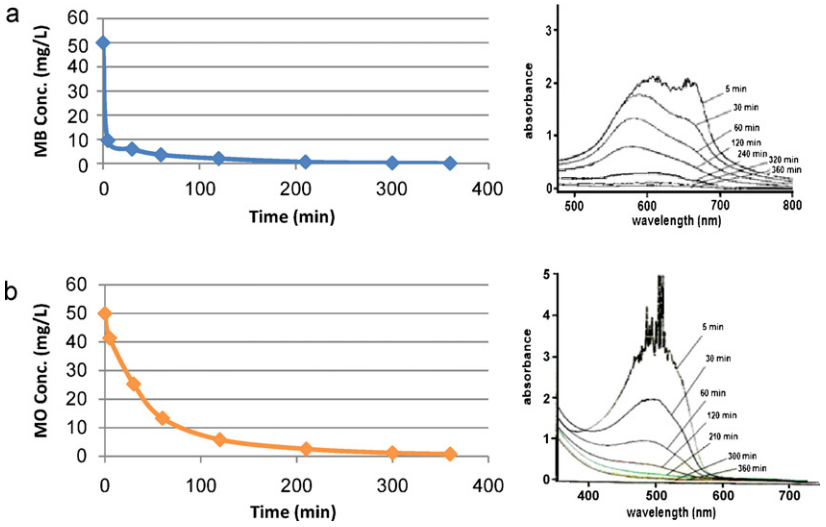

Fig. 6. Variation of dye concentration with time: (a) MB, and (b) MO. The insets show the reduction in UV–vis absorption peaks of the dyes with time.

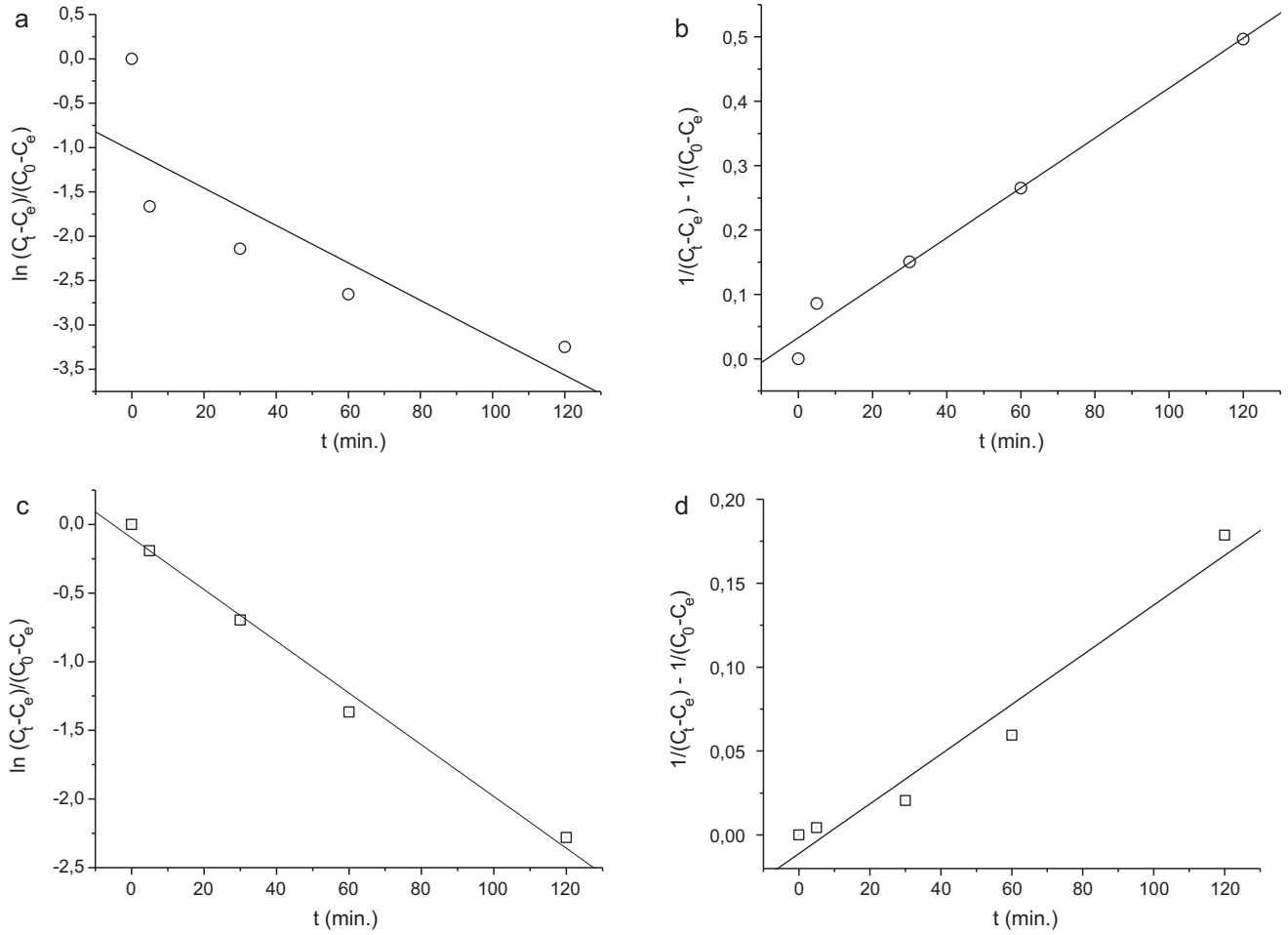

Fig. 7. Linear plots of the kinetic data: (a) first order plot for MB, (b) second order plot for MB, (c) first order plot for MO, and (d) second order plot for MO.

after 200 min for MB and 350 min for MO, under the studied conditions.

The kinetic data were fitted to first and second order rate equations. The equations are formulated by considering the driving force of removal to be proportional to the difference between the dye concentration at any time prior to equilibrium, C_t, and that at equilibrium, C_e. Hence, the first and second order rate equations for the removal of a solute C from aqueous solution might be written as [36]:

$$-\frac{dC_t}{dt} = k_1(C_t - C_e) \quad (1)$$

$$-\frac{dC_t}{dt} = k_2(C_t - C_e)^2 \quad (2)$$

where k_1 and k_2 correspond to the first and second order rate constants, respectively. Integrating the two equations under the boundary conditions $C_t = C_0$ at $t = 0$ and $C_t = C_t$ at $t = t$ yields:

$$\ln\left(\frac{C_t - C_e}{C_0 - C_e}\right) = -k_1 t \quad (3)$$

$$\frac{1}{C_t - C_e} - \frac{1}{C_0 - C_e} = k_2 t \quad (4)$$

Eqs. (3) and (4) were employed to describe the data corresponding to the pre-equilibrium stage (up to 120 min) for both dyes. The linear plots are shown in Fig. 7. The results of the linear regression analysis were used to calculate the rate constants for each case. Table 1 gives the rate constants and the corresponding linear correlation coefficients (R^2). According to the R^2 values, the removal of MB seems to fit much better to second order kinetics. This can be confirmed by the half-life test which is calculated to be 34 min based on Eq. (3) and 5.5 min based on Eq. (2). The latter value is much closer to the experimental observation as can be deduced from Fig. 6a. On the other hand, the removal of MO is found to be described somewhat better by first order kinetics. The half life value based on Eq. (3) is 42 min, while that based on Eq. (4) is about 18 min. The former value seems to be closer to the experimental value observed as 34 min, as can be seen in Fig. 6b.

At a given liquid concentration of a solute, for a fixed rate constant, the variation of the rate is more pronounced in the case of second order kinetics compared with first order. For a given rate order (first or second), the response of the rate at a given concentration will depend on the value of the rate constant. In both cases, the larger rate constant of MB reflects its faster removal kinetics.

3.2.4. *Effect of dye concentration*

The effects of MB and MO concentrations were studied over the concentration range 10–200 mg L^{-1}. Throughout the experiments, the time of contact was 6 h, which is the period required to reach

Table 1
Rate constants obtained from linear regression analysis of the data of dye removal.

Dye type	First order		Second order	
	k_1 (min^{-1})	R^2	k_2 (L mg^{-1} min^{-1})	R^2
MB	0.021	0.7060	0.0039	0.9850
MO	0.019	0.9896	0.0015	0.9623

Table 2
The percentage removal of MB and MO at different initial concentrations when GT-Fe NPs are used as a Fenton-like catalyst. C_l stands for the equilibrium liquid concentration.

Initial concentration ($mg\,L^{-1}$)	MB		MO	
	C_l ($mg\,L^{-1}$)	% Removal	C_l ($mg\,L^{-1}$)	% Removal
10.0	0.0000	100.0	0.000	100.0
25.0	0.0115	99.95	0.235	99.06
50.0	0.0266	99.95	0.548	98.90
100.0	0.0397	99.96	0.642	99.36
200.0	0.0578	99.97	0.981	99.51

equilibrium as deduced from kinetic data. As in the kinetic studies, the pH measurements showed that the system remained acidic throughout the decolorization experiments. The pH was measured at the start and end of the reactions (after 6 h of contact). For MB dye, over the studied range of concentrations, the pH values occurred in the range 3.11–3.25 at the start, and 3.23–3.30 at the end of the experiments. The measured pH range of MO was 3.19–3.33 at the start, and 3.02–3.08 at the end of the experiments. It is not certain what causes the apparent buffering effect in the system. This effect was also observed for a Fenton system containing olive mill wastewater, known to contain polyphenols along with other organics, and was referred to the formation of organic acids [29].

The calculated percentage removal at different concentrations for both dyes is given in Table 2. The removal of MB and MO appears to be almost complete over the entire concentration range, which reflects the effectiveness of the employed Fenton-like system.

To further assess the efficiency of GT-Fe NPs as a catalyst, blank experiments were performed without the addition of the material to the peroxide containing reaction mixture. The results showed less than 3% removal of the dye even in the most dilute solution.

3.3. Comparison of GT-Fe NPs with BH-Fe NPs

The degradation of MB and MO was also studied by applying iron nanoparticles produced via borohydride reduction (BH-Fe NPs) as a Fenton-like catalyst. BH-Fe NPs were prepared as described in our previous reports [1,2]. A typical SEM image and EDX spectrum of BH-Fe NPs are given in Fig. 8. The material appears to possess its characteristic chain-like morphology. An XRD pattern from the material is shown in Fig. 9. This contains reflections of iron oxides, Fe_3O_4 and FeOOH, in addition to zero valent iron, Fe^0.

The production cycle of hydroxyl radicals when iron oxide or iron oxohydroxide is used was addressed above (Section 3.2.1). A mechanism through which the Fe^0/H_2O_2 system functions has been recently suggested [10]. The production of the oxidants involves two-electron oxidation of Fe^0 followed by the Fenton reaction. First, Fe^0 is oxidized via a two electron transfer from the particle surface to H_2O_2 as shown in Eq. (iii), then the hydroxyl radical is produced by the Fenton reaction represented by Eq. (iv).

$$Fe^0 + H_2O_2 + 2H^+ \rightarrow Fe^{2+} + 2H_2O \quad \text{(iii)}$$

$$Fe^{2+} + H_2O_2 \rightarrow Fe^{3+} + OH^{\bullet} + OH^- \quad \text{(iv)}$$

Moreover, at pH values above 5, a weaker oxidant such as ferryl ion (e.g., FeO^{2+}) that is more selective than $OH^{\bullet}$ may be formed, as shown by Eq. (v) [10].

$$Fe^{2+} + H_2O_2 \rightarrow Fe(IV)(e.g., FeO^{2+}) + H_2O \quad \text{(v)}$$

Furthermore, the ferric ions produced by normal Fenton reactions can be reduced to ferrous ions by the zero valent iron metal surface [29], a step that may help sustain the production cycle of hydroxyl radical;

$$2Fe^{3+} + Fe^0 \rightarrow 3Fe^{2+} \quad \text{(vi)}$$

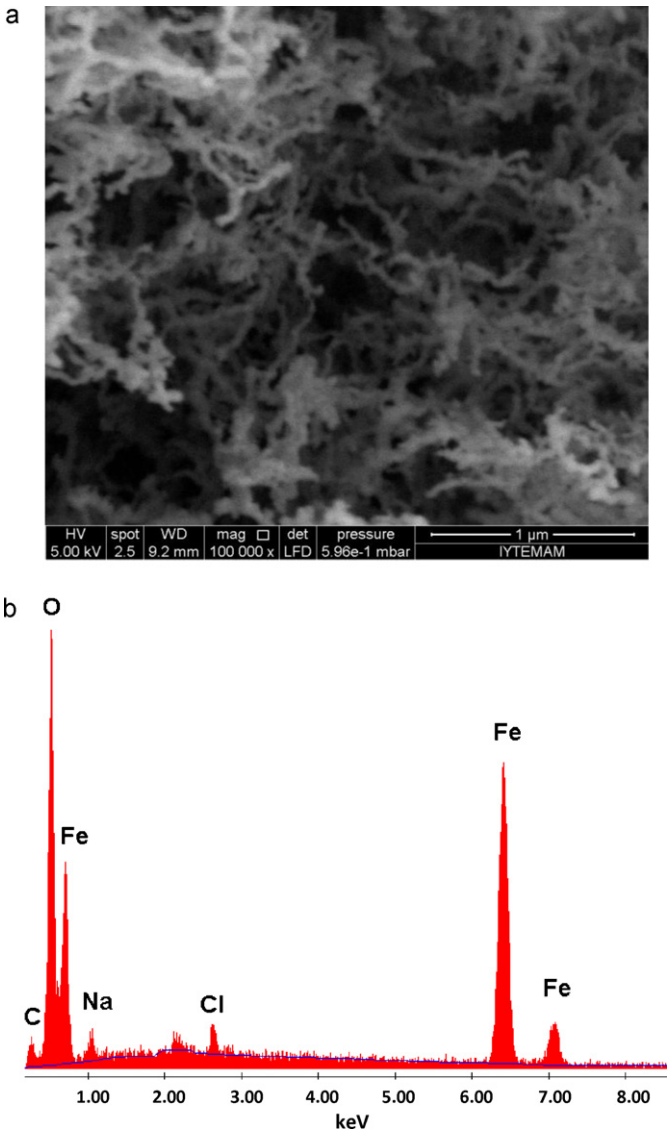

Fig. 8. (a) SEM image, and (b) EDX spectrum of BH-Fe NPs.

Overall, BH-Fe NPs appear to be less effective than GT-Fe NPs as a Fenton-like catalyst both in terms of the extent and the speed of dye removal. The obtained results are summarized in Tables 3 and 4 for MB and MO, respectively. Whereas the application of GT-Fe NPs leads to almost complete removal at all the studied dye concentrations (Table 2), the dye removal is incomplete in the case of BH-Fe NPs. At this stage, it is not clear to what extent can this be related to the chemical nature of the catalyst, or to the oxidation state of iron. A more detailed investigation is necessary to address the topic.

The removal of MB appears to be comparatively much better than that of MO in terms of its extent of removal when BH-Fe NPs is used as a Fenton-like catalyst. The kinetic data of MB and MO showed poor correlations with both first and second order models (Eqs. (3) and (4)) at the initial dye concentration of 10 $mg\,L^{-1}$. At the initial concentration of 100 $mg\,L^{-1}$, the correlation is somewhat fair, and it suggests that the removal of MB proceeds faster than

Table 3
Kinetic and equilibrium data corresponding to removal of MB when borohydride-reduced Fe (BH-Fe NPs) is used as a Fenton-like catalyst.

Initial concentration (mg L^{-1})	% Removal at equilibrium	First order		Second order	
		k_1 (min^{-1})	R^2	k_2 (L mg^{-1} min^{-1})	R^2
10	96.3	0.013	0.9506	0.0078	0.9333
100	86.6	0.016	0.9997	0.00030	0.9922

Table 4
Kinetic and equilibrium data corresponding to removal of MO when borohydride-reduced Fe (BH-Fe NPs) is used as a Fenton-like catalyst.

Initial concentration (mg L^{-1})	% Removal at equilibrium	First order		Second order	
		k_1 (min^{-1})	R^2	k_2 (L mg^{-1} min^{-1})	R^2
10	61.6	0.0017	0.9240	0.0007	0.9771
100	47.1	0.0013	0.9022	0.00005	0.9737

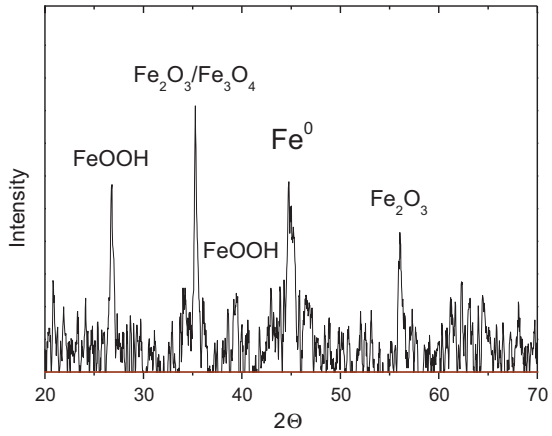

Fig. 9. XRD pattern of BH-Fe NPs.

that of MO, which is roughly inline with the results obtained upon employing GT-Fe NPs as a Fenton-like catalyst.

Nevertheless, the reported results must not undermine the effectiveness of BH-Fe NPs in dye removal. Preliminary data of our ongoing experiments suggest that BH-Fe NPs would be much more effective than GT-Fe NPs when used directly (not as a Fenton-like catalyst; without H_2O_2) to catalyze dye degradation/sorption. This topic is still under investigation and will hopefully be addressed in a future publication.

4. Conclusions

Iron nanoparticles rich with iron oxide/oxohydroxide can be readily prepared using green tea extract. The material seems to possess different morphology and structural characteristics than iron nanoparticles produced by reduction with sodium borohydride.

As a Fenton-like catalyst, GT-Fe NPs demonstrated impressive removal capabilities towards both of MB and MO, in terms of the extent of removal and the kinetics. Compared with BH-Fe NPs, GT-Fe NPs showed higher dye removal percentages and faster kinetics when used as a Fenton-like catalyst.

Acknowledgments

This research was financed by Birzeit University through project no. 211006. The authors thank Mr. Ibrahim Shalash and Mr. Ahmad Amer of the Department of Chemistry, Birzeit University for their help in supplying the needed chemicals and in recording the FTIR spectra. The authors thank the Center of Materials Research at Izmir Institute of Technology for help with the SEM/EDX and XRD characterization.

References

[1] N. Efecan, T. Shahwan, A.E. Eroğlu, I. Lieberwirth, Characterization of the uptake of aqueous Ni^{2+} ions on nanoparticles of zero-valent iron (nZVI), Desalination 249 (2009) 1048–1054.
[2] Ç. Üzüm, T. Shahwan, A.E. Eroğlu, I. Lieberwirth, T.B. Scott, K.R. Hallam, Application of zero-valent iron nanoparticles for the removal of aqueous Co^{2+} ions under various experimental conditions, Chem. Eng. J. 144 (2008) 213–220.
[3] H.-Y. Shu, M.-C. Chang, H.-H. Yu, W.-H. Chen, Reduction of an azo dye Acid Black 24 solution using synthesized nanoscale zerovalent iron particles, J. Colloid Interface Sci. 314 (2007) 89–97.
[4] Y.-T. Wei, S.-C. Wu, C.-M. Chou, C.-H. Che, S.-M. Tsai, H.-L. Lien, Influence of nanoscale zero-valent iron on geochemical properties of groundwater and vinyl chloride degradation: a field case study, Water Res. 44 (2010) 131–140.
[5] Y. Liu, T. Phenrat, G.V. Lowry, Effect of TCE concentration and dissolved groundwater solutes on NZVI-promoted TCE dechlorination and H_2 evolution, Environ. Sci. Technol. 41 (2007) 7881–7887.
[6] Y. Liu, G.V. Lowry, Effect of particle age (Fe^0 content) and solution pH on nZVI reactivity: H_2 evolution and TCE dechlorination, Environ. Sci. Technol. 40 (2006) 6085–6090.
[7] O. Çelebi, Ç. Üzüm, T. Shahwan, H.N. Erten, A radiotracer study of the adsorption behavior of aqueous Ba^{2+} ions on nanoparticles of zero-valent iron, J. Hazard. Mater. 148 (2007) 761–767.
[8] W. Yan, A.A. Herzing, C.J. Kiely, W.-X. Zhang, Nanoscale zero-valent iron (nZVI): aspects of the core–shell structure and reactions with inorganic species in water, J. Contam. Hydrol. 118 (2010) 96–104.
[9] S. Shin, H. Yoon, J. Jang, Polymer-encapsulated iron oxide nanoparticles as highly efficient Fenton catalysts, Catal. Commun. 10 (2008) 178–182.
[10] L. Xu, J. Wang, A heterogeneous Fenton-like system with nanoparticulate zero-valent iron for removal of 4-chloro-3-methyl phenol, J. Hazard. Mater. 186 (2011) 256–264.
[11] G. Zelmanov, R. Semiat, Iron(3) oxide-based nanoparticles as catalysts in advanced organic aqueous oxidation, Water Res. 42 (2008) 492–498.
[12] Y.-P. Sun, X.-Q. Li, J. Cao, W.-X. Zhang, H.P. Wang, Characterization of zero-valent iron nanoparticles, Adv. Colloid Interface Sci. 120 (2006) 47–56.
[13] Y.-P. Sun, X.-Q. Li, W.-X. Zhang, H.P. Wang, A method for the preparation of stable dispersion of zero-valent iron nanoparticles, Colloids Surf. A 308 (2007) 60–66.
[14] H.-Y. Shu, M.-C. Chang, C.-C. Chen, P.-E. Chen, Using resin supported nano zero-valent iron particles for decoloration of Acid Blue 113 azo dye solution, J. Hazard. Mater. 184 (2010) 499–505.
[15] Ç. Üzüm, T. Shahwan, A.E. Eroğlu, K.R. Hallam, T.B. Scott, I. Lieberwirth, Synthesis and characterization of kaolinite-supported zero-valent iron nanoparticles and their application for the removal of aqueous Cu^{2+} and Co^{2+} ions, Appl. Clay Sci. 43 (2009) 172–181.
[16] W. Wang, M. Zhou, Q. Mao, J. Yue, X. Wang, Novel NaY zeolite-supported nanoscale zero-valent iron as an efficient heterogeneous Fenton catalyst, Catal. Commun. 11 (2010) 937–941.
[17] G. Hoag, J. Collins, J. Holcomb, J. Hoag, M. Nadagouda, R. Varma, Degradation of bromothylmol blue by 'greener' nano-scale zero-valent iron synthesized using tea polyphenols, J. Mater. Chem. 19 (2009) 8671–8677.
[18] M.N. Nadagouda, A.B. Castle, R.C. Murdock, S.M. Hussain, R.S. Varma, In vitro biocompatibility of nanoscale zerovalent iron particles (NZVI) synthesized using tea polyphenols, Green Chem. 12 (2010) 114–122.
[19] E.C. Njagi, H. Huang, L. Stafford, H. Genuino, H.M. Galindo, J.B. Collins, G.E. Hoag, S.L. Suib, Biosynthesis of iron and silver nanoparticles at room temperature using aqueous Sorghum Bran extracts, Langmuir 27 (2011) 264–271.
[20] B.-H. Moon, Y.-B. Park, K.-H. Park, Fenton oxidation of Orange II by pre-reduction using nanoscale zero-valent iron, Desalination 268 (2011) 249–252.

[21] S. Nasrazadani, H. Namduri, Study of phase transformation in iron oxides using laser induced breakdown spectroscopy, Spectrochim. Acta Part B 61 (2006) 565–571.
[22] D.K. Lee, Y.S. Kang, Preparation and characterization of magnetic nanoparticles by γ-irradiation, Mater. Sci. Eng.: C 24 (2004) 107–111.
[23] M. Aronniemi, J. Sainio, J. Lahtinen, XPS study on the correlation between chemical state and oxygen-sensing properties of an iron oxide thin film, Appl. Surf. Sci. 253 (2007) 9476–9482.
[24] H. Abdel-Samad, P.R. Watson, An XPS study of the adsorption of lead on goethite (α-FeOOH), Appl. Surf. Sci. 136 (1998) 46–54.
[25] J.H. Linn, W.E. Swartz Jr., An XPS study of the water adsorption/desorption characteristics of transition metal oxide surfaces: microelectronic implications, Appl. Surf. Sci. 20 (1984) 154–166.
[26] E. Paparazzo, XPS analysis of iron aluminum oxide systems, Appl. Surf. Sci. 25 (1986) 1–12.
[27] R. Silverstein, G. Bassler, T. Morrill, Spectrometric Identification of Organic Compounds, 5th ed., Courier Companies Inc., Canada, 1991.
[28] X. Xue, K. Hanna, N. Deng, Fenton-like oxidation of Rhodamine B in the presence of two types of iron (II, III) oxide, J. Hazard. Mater. 166 (2009) 407–414.
[29] M. Kallel, C. Belaid, T. Mechichi, M. Ksibi, B. Elleuch, Removal of organic load and phenolic compounds from olive mill wastewater by Fenton oxidation with zero-valent iron, Chem. Eng. J. 150 (2009) 391–395.
[30] R.J. Watts, M.K. Foget, S.H. Kong, A.L. Teel, Hydrogen peroxide decomposition in model subsurface systems, J. Hazard. Mater. 69 (1999) 229–243.
[31] K. Imamura, E. Ikeda, T. Nagayasu, T. Sakiyama, K. Nakanishi, Adsorption behavior of methylene blue and its congeners on a stainless steel surface, J. Colloid Interface Sci. 245 (2002) 50–57.
[32] G. Pashetti, A. Telke, D. Kalyani, S. Govindwar, Decoloration and detoxification of sulfonated azo dye methyl orange, J. Hazard. Mater. 176 (2010) 503–509.
[33] G.S. Singhal, E. Rabinowitch, Changes in the absorption spectrum of methylene blue with pH, J. Phys. Chem. 71 (1967) 3347–3349.
[34] J. Oakes, P. Gratton, Kinetic investigations of the oxidation of Methyl Orange and substituted arylazonaphthol dyes by peracids in aqueous solution, J. Chem. Soc.: Perkin Trans. 2 (1998) 2563–2568.
[35] W.G. Kuo, Decolorizing dye wastewater with Fenton's reagent, Water Res. 26 (1992) 881–886.
[36] T. Shahwan, Ç. Üzüm, A.E. Eroğlu, I. Lieberwirth, Synthesis and characterization of bentonite/iron nanoparticles and their application as adsorbent of cobalt ions, Appl. Clay Sci. 47 (2010) 257–262.